Polarization-selective computer-generated holograms: design, fabrication, and applications

Fang Xu, Joseph E. Ford, and Yeshayahu Fainman

We constructed polarization-selective computer-generated holograms that apply an independent phase profile during readout by horizontal and vertical light polarizations. These elements are composed of two surface-relief-etched birefringent substrates joined face to face. We describe the design methodology for arbitrary birefringent substrate and gap materials. We show how these holograms are fabricated with standard microelectronics technology and discuss the effects of etching and alignment errors on performance. We demonstrated a diffraction efficiency of 60% with a polarization contrast ratio of >100:1 using a multilevel phase hologram made from two birefringent lithium niobate substrates. We also showed that a single-layer SiO_2 thin-film antireflection coating on all surfaces can reduce reflections from the high-index substrates without significant effect on hologram performance. We also consider some possible applications of this technology and demonstrate experimentally a dual focal-length lens and a self-interconnecting binary 2×2 polarization switch.

Key words: Polarization-selective diffractive element, computer-generated kinoforms, optoelectronic packaging, optical interconnects, photonic switching, image processing.

1. Introduction

Computer-generated holograms (CGH's) have proven useful for numerous applications such as aberration correction, optical filtering, free-space optical interconnections, and the packaging of compact optoelectronics systems. CGH's can be fabricated with standard microelectronics lithography and etching techniques, which are accurate, cost effective, and reproducible. Conventional CGH optical elements are fabricated either with a simple-patterned transmission mask (amplitude CGH) or with surface-relief etching of an isotropic substrate (phase or kinoform CGH). Both are normally insensitive to readout light polarization. However, a polarization-selective CGH, which appears completely different at the two orthogonal linear polarizations, could further extend the number and type of CGH applications. A polarization-selective CGH would effectively separate the readout light by polarization, act independently on each path, and recombine the beams, as shown in Fig. 1. This paper describes the design, fabrication, and testing of phase-only CGH's made polarization selective by fabrication in birefringent substrates. This type of element may have an important role in building compact optoelectronic components and systems. We demonstrate how such elements can be used to make an electrically controlled lens and a self-interconnecting binary 2×2 polarization switch. The role of polarization-selective CGH's in building compact optoelectronic components and systems is also discussed.

Polarization-sensitive volume and surface-relief holograms have been optically recorded in organic dyes,[1] photorefractive crystals,[2] and dichromated gelatin.[3] Optically recorded holograms normally have high spatial resolution and are relatively simple to produce. However, they lack the flexibility of a phase-only CGH, which is a surface grating used in constructing an arbitrary phase function. For example, a CGH might realistically be designed to interconnect a large array of input beams to multiple output locations that at the same time compensates for local aberrations. In addition, CGH's fabricated by surface profile etching cannot shrink or swell, so their performance is reliable under a variety of environmental conditions.

High spatial frequency surface-relief gratings, where the grating period is comparable to or less than the optical readout wavelength, have been used to make

When this work was performed, the authors were with the Department of Electrical and Computer Engineering, University of California, San Diego, La Jolla, California 92093-0407. J. E. Ford is now with AT&T Bell Laboratories, 101 Crawfords Corner Road, Homdel, New Jersey 07733-0303.

Received 18 February 1994; revised manuscript received 25 July 1994.

0003-6935/95/020256-11$06.00/0.

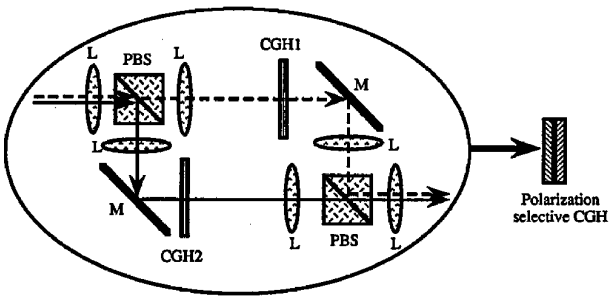

Fig. 1. Effective function of a polarization-selective CGH: L's, lenses; PBS's, polarizing beam splitters; M's, mirrors.

planar-polarizing beam splitters.[4,5] Ohba *et al.* used proton exchange in lithium niobate to create a birefringent polarizing grating.[6] Also, polarization-selective amplitude-modulated CGH's have been made by laser bleaching of thin polarizing films.[7] Two of these films in contact provided a contrast ratio of 15–30 to 1 between two orthogonal polarizations, with a diffraction efficiency of ~9%.

Our approach permits recording of a polarization-selective multilevel phase CGH with a large polarization contrast ratio and a diffraction efficiency theoretically approaching 100%. The element, called a BCGH (for birefringent CGH), is composed of two substrates, at least one of which is birefringent. The substrates are both etched with a surface-relief patterns, then joined face to face to yield a single element with the etched surfaces on the interior. In Sections 2 and 3 we introduce the principle, the analysis, and the design procedures of a BCGH. In Section 4 we describe BCGH fabrication. In Section 5 we describe our experimental BCGH evaluation and discuss the effects of fabrication errors on performances; potential applications are also described in this section. We conclude with a summary and some future directions in Section 6.

2. Basic Principles and Analysis

A phase CGH consists of a two-dimensional array of pixels, where each pixel has an associated phase relative to the others. The absolute phase delay, corresponding, for example, to the thickness of the hologram substrate, is normally not important. In a kinoform hologram the surface of an isotropic substrate is shaped so that the optical path through each pixel creates the desired phase delay. This surface profile can be created either by deposition or by removal of material from an initially planar substrate. The maximum possible diffraction efficiency from a kinoform hologram depends on the accuracy with which the theoretically continuous phase values are actually fabricated: 40.5% for 2-level (binary) phase, 81.1% for 4-level phase, 95.0% for 8-level phase, 98.7% for 16-level phase, and 99.7% for 32-level phase.[8]

Standard lithographic techniques used for microelectronic fabrication can be used to create an accurate multilevel phase profile with high spatial resolution. Binary phase patterns can be fabricated by patterning and etching of a photoresist-covered substrate. A second patterning and etching process yields four phase levels, a third yields eight phase levels, and so on. The diffracted output from computer-generated holograms is normally independent of input polarization. Holograms with the grating period comparable to or smaller than the readout wavelength[9] and metallic gratings with large periods but small feature sizes[10] do show polarization selectivity. In these cases the input polarization can affect the intensity diffracted into different output orders. However, our goal is a single diffractive element with independent, efficient reconstructions for each of the two orthogonal linear polarizations.

If a diffractive optical element with independent impulse responses for two orthogonal linear polarizations is needed, then two independent phase functions must be implemented by the element. For each polarization each pixel should have the necessary phase relative to the rest of the pixels. Equivalently we can say that each pixel should introduce the desired phase angle between the ordinary and extraordinary polarization inputs as well as the correct phase relative to the rest of the array at either polarization. If we fabricated a conventional single-substrate CGH in a birefringent substrate, we could compute and etch the surface to obtain the correct phase delay for only one of the two possible independent input polarizations. The hologram seen by the orthogonal polarization would in general be incorrect. We therefore introduce a second phase-only CGH fabricated in a different substrate, and we place the two surface-relief patterns in contact, as shown in Fig. 2. If the gap between the two substrates and the etch depths are comparable to the feature size, then the two surface profiles lie in essentially the same optical plane. These two surface-relief patterns give us two degrees of freedom, the independent etch depths d_1 and d_2, to satisfy the two requirements of the relative phase difference among every pixel and phase difference between the two orthogonal polarizations inside each pixel. In general, two substrates can be made of two different birefringent crystals. The gap media can also be birefringent [i.e., liquid crystal (LC)] but would normally be isotropic (i.e., air).

From Fig. 2 we can see that the optical path differences L_o and L_e corresponding to ordinary and

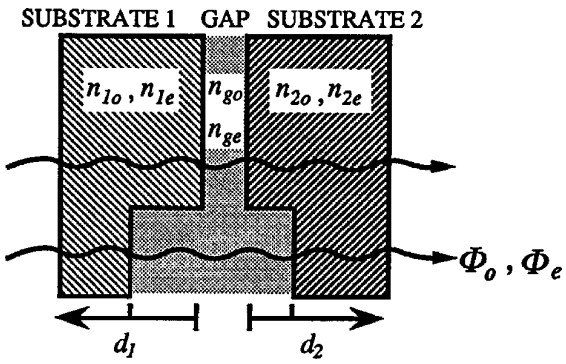

Fig. 2. Geometry of a single pixel in the BCGH.

extraordinary polarized light propagating through an etched pixel relative to an unetched pixel are given by

$$(n_{1e} - n_{ge})d_1 + (n_{2e} - n_{ge})d_2 = L_e, \quad (1a)$$

$$(n_{1o} - n_{go})d_1 + (n_{2o} - n_{go})d_2 = L_o, \quad (1b)$$

where d_1 and d_2 are the etch depths in the first and second substrates, n_{1o} and n_{1e} are the refractive indices of the first birefringent substrate for ordinary and extraordinary polarizations, n_{2o} and n_{2e} are the refractive indices of the second birefringent substrate for ordinary and extraordinary polarizations, and n_{go} and n_{ge} are the refractive indices of the birefringent gap media for ordinary and extraordinary polarizations.

Equations (1) can also be rewritten in the form of phase differences,

$$(n_{1e} - n_{ge})\phi_1 + (n_{2e} - n_{ge})\phi_2 = \Phi_e, \quad (2a)$$

$$(n_{1o} - n_{go})\phi_1 + (n_{2o} - n_{go})\phi_2 = \Phi_o, \quad (2b)$$

where

$$\phi_1 = k_0 d_1 = (2\pi/\lambda_0)d_1, \quad \phi_2 = k_0 d_2 = (2\pi/\lambda_0)d_2,$$
$$\Phi_e = k_0 L_e = (2\pi/\lambda_0)L_e, \quad \Phi_o = k_0 L_o = (2\pi/\lambda_0)L_o. \quad (3)$$

Here ϕ_1 and ϕ_2 are the phase delays corresponding to the etch depths d_1 and d_2, respectively, for the optical wave propagating in a vacuum. Φ_o and Φ_e are the phases acquired by ordinary- and extraordinary-polarized optical waves upon propagation of lengths L_o and L_e, respectively, and λ_0 is the wavelength of the optical wave in a vacuum. To realize different and independent impulse responses for the two orthogonal linear polarizations, we must ensure that Eqs. 2(a) and 2(b) are linearly independent, i.e., the determinant of coefficients matrix is different from zero:

$$\begin{vmatrix} n_{1e} - n_{ge} & n_{2e} - n_{ge} \\ n_{1o} - n_{go} & n_{2o} - n_{go} \end{vmatrix} \neq 0. \quad (4)$$

When both substrates are identical, so that $n_{1o} = n_{2o} = n_o$ and $n_{1e} = n_{2e} = n_e$, inequality (4) cannot be satisfied. Therefore we require that either $n_{1o} \neq n_{2o}$ or $n_{1e} \neq n_{2e}$.

In the following we will consider three special cases of the general BCGH configurations that can satisfy inequality (4): (i) an isotropic gap between a birefringent and an isotropic substrate, (ii) an isotropic gap between two different birefringent substrates, and (iii) a birefringent gap medium between two different birefringent substrates:

(i) *Isotropic gap medium between a birefringent substrate and an isotropic substrate.* Assuming $n_{go} = n_{ge} = n_g$ and $n_{2o} = n_{2e} = n_2$, we can rewrite inequality (4) as

$$(n_{1e} - n_{1o})(n_2 - n_g) \neq 0. \quad (5)$$

This shows that one of the substrates must be birefringent and that the gap medium and the isotropic substrate cannot have the same refractive indices. The phase diagram for this case is shown in Fig. 3(a). For example, if the desired phase delays for ordinary and extraordinary polarizations at a pixel are $\pi/2$ and $\pi/3$, respectively, then the etch in the first birefringent substrate introduces the desired phase difference $\pi/6$ between the two polarizations, while the second etch in the isotropic substrate sets the relative phase relation with other pixels for both polarizations. Because the phase difference between the two orthogonal polarizations is introduced only by the first (birefringent) substrate, the etch depth in this case may be large.

(ii) *Isotropic gap medium between two birefringent substrates.* Assuming $n_{go} = n_{ge} = n_g$ and under this assumption, Inequality (4) can be written as

$$(n_{1e} - n_g)(n_{2o} - n_g) - (n_{2e} - n_g)(n_{1o} - n_g) \neq 0 \quad (6)$$

or

$$(n_{1e}n_{2o} - n_{1o}n_{2e}) + n_g[(n_{1o} - n_{1e}) - (n_{2o} - n_{2e})] \neq 0. \quad (6')$$

Besides the requirement that the two substrates cannot have the same refractive indices for the same polarization, there is no other constraint required in this case. The phase diagram under this configuration is shown in Fig. 3(b). Compared with the previous case, both substrates contribute to the desired $\pi/6$ phase difference between the two orthogonal polarizations as well as to the relative phase relation with respect to other pixels for the two orthogonal polarizations. Because the phase difference between the orthogonal polarizations is introduced by both substrates, the etch depth in each substrate will be smaller. Furthermore, we can use

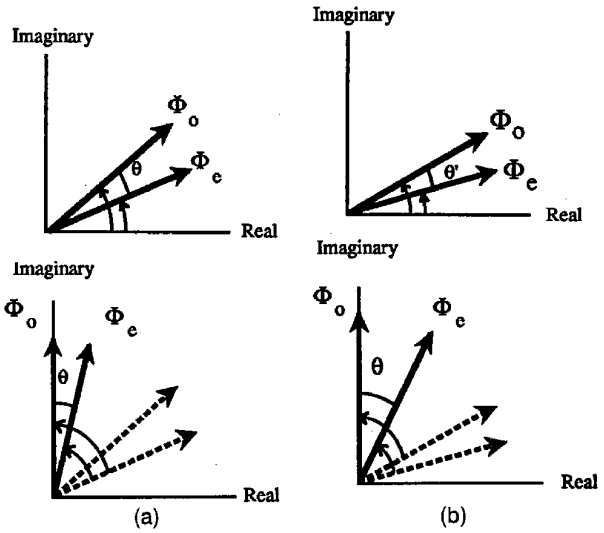

Fig. 3. Phasor diagrams, of a BCGH constructed of (a) a birefringent (upper) and an isotropic (lower) substrate and (b) two birefringent substrates (the first and second substrates, respectively). Both cases (a) and (b) assume an isotropic gap medium.

the same birefringent crystal for both substrates provided that we rotate their crystal axes by 90° with respect to each other. With this configuration we can reduce fabrication complexity and time, as will be discussed in greater detail in Section 3.

(iii) *Anisotropic gap medium.* With this special configuration we can use different combinations of substrates as long as at least one index is different. This approach will permit a further reduction of the required etch depth with two birefringent substrates because both substrates and the gap medium contribute to the required phase difference between the two orthogonal polarizations. The main disadvantage lies in the complexity of aligning the crystal axis of the gap medium. The phase diagram of a birefringent gap medium between two isotropic substrates is similar to that of Fig. 3(b). This approach also introduces the possibility of direct electrical control of the gap material's birefringence, for example, with a liquid crystal between transparent electrodes on the substrate surfaces. Such an arrangement might be exploited to create a switching holographic element.

In our experiments we chose to use the same birefringent crystal for both substrates of the BCGH, rotating the optic axis of the second substrate 90° with respect to the first. For such an arrangement the refractive indices of the substrates are given by

$$n_{2e} = n_{1o} = n_o, \tag{7a}$$

$$n_{2o} = n_{1e} = n_e, \tag{7b}$$

Also, in practice the gap medium is isotropic with refractive index n_g; then Eqs. (2) can be written as

$$\begin{aligned}(n_e - n_g)\phi_1 + (n_o - n_g)\phi_2 &= \Phi_e,\\ (n_o - n_g)\phi_1 + (n_e - n_g)\phi_2 &= \Phi_o.\end{aligned} \tag{8}$$

Unlike single-substrate holograms, we have to consider the free-space propagation of light in the gap between the two surface-relief diffractive structures. Usually the thickness of the gap between the two substrates in unetched regions can be negligibly small (i.e., the gap between the two substrates is of the order of the substrate flatness, which for optical surfaces is usually less than a fraction of a wavelength). In diffractive optics the single pixel size is of the order of a few micrometers (in our experiments the pixel size is 10 μm). We can therefore neglect interference between adjacent pixels so that analysis with geometrical optics is justified, provided that the etch depths are not larger than the feature size.

3. Birefringent Computer-Generated-Hologram Design

One of the important initial steps in constructing a multiphase-level diffractive optical element is to generate a set of masks with computer-synthesized data. The method of generating masks for conventional single-substrate diffractive optical element (described in Ref. 8) consists of the following: (i) starting with the desired phase function $\Phi(x, y)$ and generating a new discontinuous function $\Phi'(x, y)$, which is $\Phi(x, y)$ modulo 2π, then (ii) choosing the number of phase-quantization levels depending on the desired diffraction efficiency, and (iii) quantizing $\Phi'(x, y)$ to generate the binary transmission masks to fabricate the quantized multiphase-level version $\Phi_q(x, y)$. In general, $\log_2 N$ mask transfers and etches are needed to fabricate an N-phase-level single-substrate CGH.

We need the BCGH to implement two independent phase functions $\Phi_o(x, y)$ and $\Phi_e(x, y)$ for the ordinary and extraordinary polarizations, respectively. From Eqs. (2) and (3) we obtain the required etch depths

$$\begin{aligned} d_1 &= \frac{1}{k_0}\frac{\begin{vmatrix}\Phi_e & n_{2e} - n_{ge}\\ \Phi_o & n_{2o} - n_{go}\end{vmatrix}}{\begin{vmatrix}n_{1e} - n_{ge} & n_{2e} - n_{ge}\\ n_{1o} - n_{go} & n_{2o} - n_{go}\end{vmatrix}}\\ &= \frac{1}{k_0}\frac{(n_{2o} - n_{go})\Phi_e - (n_{2e} - n_{ge})\Phi_o}{(n_{1e} - n_{ge})(n_{2o} - n_{go}) - (n_{1o} - n_{go})(n_{2e} - n_{ge})},\\ d_2 &= \frac{1}{k_0}\frac{\begin{vmatrix}n_{1e} - n_{ge} & \Phi_e\\ n_{1o} - n_{go} & \Phi_o\end{vmatrix}}{\begin{vmatrix}n_{1e} - n_{ge} & n_{2e} - n_{ge}\\ n_{1o} - n_{go} & n_{2o} - n_{go}\end{vmatrix}}\\ &= \frac{1}{k_0}\frac{(n_{1e} - n_{ge})\Phi_o - (n_{1o} - n_{go})\Phi_e}{(n_{1e} - n_{ge})(n_{2o} - n_{go}) - (n_{1o} - n_{go})(n_{2e} - n_{ge})}. \end{aligned} \tag{9}$$

For N phase-quantization levels the phase functions Φ_o and Φ_e will be transferred into their discrete-valued versions Φ_{oq} and Φ_{eq}, respectively. Φ_{oq} and Φ_{eq} will take one of the following values:

$$\begin{aligned}\Phi_{oq} \in \Big\{0, \frac{2\pi}{N}, 2\times\frac{2\pi}{N}, 3\times\frac{2\pi}{N}, \ldots, N_{oq}\\ \times\frac{2\pi}{N}, \ldots, (N-1)\times\frac{2\pi}{N}\Big\},\\ \Phi_{eq} \in \Big\{0, \frac{2\pi}{N}, 2\times\frac{2\pi}{N}, 3\times\frac{2\pi}{N}, \ldots, N_{eq}\\ \times\frac{2\pi}{N}, \ldots, (N-1)\times\frac{2\pi}{N}\Big\},\end{aligned} \tag{10}$$

where N_{oq} and N_{eq} are integers varying from 0 to $N - 1$. Therefore we can rewrite Eqs. (9) in its discrete form:

$$\begin{aligned} d_{1q} &= \frac{1}{k_0}\frac{(n_{2o} - n_{go})\Phi_{eq} - (n_{2e} - n_{ge})\Phi_{oq}}{(n_{1e} - n_{ge})(n_{2o} - n_{go}) - (n_{1o} - n_{go})(n_{2e} - n_{ge})}\\ &= \frac{\lambda}{N}\frac{(n_{2o} - n_{go})N_{eq} - (n_{2e} - n_{ge})N_{oq}}{(n_{1e} - n_{ge})(n_{2o} - n_{go}) - (n_{1o} - n_{go})(n_{2e} - n_{ge})},\\ d_{2q} &= \frac{1}{k_0}\frac{(n_{1e} - n_{ge})\Phi_{oq} - (n_{1o} - n_{go})\Phi_{eq}}{(n_{1e} - n_{ge})(n_{2o} - n_{go}) - (n_{1o} - n_{go})(n_{2e} - n_{ge})}\\ &= \frac{\lambda}{N}\frac{(n_{1e} - n_{ge})N_{oq} - (n_{1o} - n_{go})N_{eq}}{(n_{1e} - n_{ge})(n_{2o} - n_{go}) - (n_{1o} - n_{go})(n_{2e} - n_{ge})}. \end{aligned} \tag{11}$$

We can define four fundamental etch-depth increments:

$$s = \frac{1}{N}\frac{\lambda_0(n_{1e} - n_{ge})}{[(n_{1e} - n_{ge})(n_{2o} - n_{go}) - (n_{1o} - n_{go})(n_{2e} - n_{ge})]},$$

$$t = \frac{1}{N}\frac{\lambda_0(n_{1o} - n_{go})}{[(n_{1e} - n_{ge})(n_{2o} - n_{go}) - (n_{1o} - n_{go})(n_{2e} - n_{ge})]},$$

$$p = \frac{1}{N}\frac{\lambda_0(n_{2e} - n_{ge})}{[(n_{1e} - n_{ge})(n_{2o} - n_{go}) - (n_{1o} - n_{go})(n_{2e} - n_{ge})]},$$

$$q = \frac{1}{N}\frac{\lambda_0(n_{2o} - n_{go})}{[(n_{1e} - n_{ge})(n_{2o} - n_{go}) - (n_{1o} - n_{go})(n_{2e} - n_{ge})]}, \quad (12)$$

Equations (11) then can be rewritten in a simple quantized form in terms of the fundamental etch-depth increments defined in Eqs. (12):

$$d_{1q} = N_{eq}t - N_{oq}s, \quad (13a)$$

$$d_{2q} = N_{oq}p - N_{eq}q. \quad (13b)$$

Because N_{oq} and N_{eq} are integers varying from 0 to $N - 1$, the corresponding quantized etch depths have, in general, a total of N^2 different surface-relief levels in each substrate.

Notice that the quantized values d_{1q} and d_{2q} are depths etched into the flat surface, and from practical fabrication considerations these depths must be positive. To ensure such a fabrication-imposed constraint, we simply add a constant $(N - 1)s$ to both sides of Eq. 13(a) and add a constant $(N - 1)q$ to both sides of Eq. 13(b) (because in diffractive optics, constant phase added to all pixels is of no concern). Equations (13) can then be rewritten as

$$d'_{1q} = N_{eq}t + (N - 1 - N_{oq})s,$$

$$d'_{2q} = N_{oq}p + (N - 1 - N_{eq})q, \quad (14)$$

Where d'_{1q} and d'_{2q} are the corresponding positive etch depths for the two substrates, respectively. Here we simply assume all four etch-depth increments in Eqs. (12) are positive; therefore both d'_{1q} and d'_{2q} are positive. If the substrate indices do not satisfy this assumption, we can still add constants to both sides of Eqs. 13(a) and 13(b) to make the actual etch depths not less than zero.

In our experiments we choose to make the BCGH with an isotropic gap medium of index n_g between two substrates made of the same uniaxial material but with crystal axes rotated by 90° with respect to each other [as in Eqs. 7(a) and 7(b)]. For this special case the four fundamental etch-depth increments are reduced to two,

$$s = q = \frac{1}{N}\frac{\lambda_0(n_e - n_g)}{[(n_e - n_g)^2 - (n_o - n_g)^2]},$$

$$t = p = \frac{1}{N}\frac{\lambda_0(n_o - n_g)}{[(n_e - n_g)^2 - (n_o - n_g)^2]}, \quad (15)$$

and the required discrete etch depths can be expressed as

$$d'_{1q} = N_{eq}t + (N - 1 - N_{oq})s,$$

$$d'_{2q} = N_{oq}t + (N - 1 - N_{eq})s. \quad (16)$$

According to Eqs. (16), d'_{1q} and d'_{2q} are both linear combinations of two independent variables s and t. We can design two sets of the corresponding electron-beam (e-beam) masks for implementing the quantized multilevel etches d'_{1q} and d'_{2q}. To fabricate an N-phase-level BCGH, we need $\log_2 N$ e-beam masks for implementing each term of Eqs. (16). Therefore a total of $4 \log_2 N$ e-beam masks are needed to implement d'_{1q} and d'_{2q}. This is four times as many masks as for constructing a single-substrate diffractive optical element. However, because we are using the same birefringent material for the two substrates of BCGH, we can fabricate both substrates simultaneously with a total number of $2 \log_2 N$ mask and etch steps.

4. Birefringent Computer-Generated-Hologram Fabrication Procedure

The birefringent material we used to fabricate the BCGH elements was a lithium niobate ($LiNbO_3$) crystal with its crystal optic axis parallel to the substrate surface. We chose lithium niobate because of its high optical quality, reasonable cost, and relatively large birefringence ($n_o = 2.3325$ and $n_e = 2.2422$ at $\lambda = 514.5$ nm).[11] The substrates used were 1-mm-thick Y-cut crystal wafers of 3-in. (76-mm) diameter, optically polished on both surfaces with surface flatness of less than 0.16 μm over a length of 1 cm.

In general, $4 \log_2 N$ e-beam masks are needed to make an N-phase-level BCGH. To simplify BCGH fabrication, we patterned and etched both substrates simultaneously on the same lithium niobate wafer, cut into a 1 in. × 2 in. (25 mm × 51 mm) rectangle. The pattern masks for both substrates are written on the same e-beam plate, but the corresponding two patterns are rotated by 90° with respect to each other. After the etching was complete, the wafer was cut into two and assembled with orthogonal optical axes. With this approach the total number of required distinct etches was halved to $2 \log_2 N$. Table 1 shows the etch depths required for binary and four-level phase BCGH's fabricated from twin lithium niobate substrates. For a N-phase-level BCGH the required surface-relief profile has, in general, N^2 levels instead of the N levels of a conventional single-substrate diffractive optical element.

The pattern masks for BCGH were made by e-beam lithography. The BCGH element itself was fabricated with standard microelectronics techniques: microlithography to transfer the patterns onto the substrate and ion-beam etching to obtain the surface-relief patterns in the substrate.[12] A reactive-ion-beam etching machine (MICROETCH from VEECO) was used in the etching processing with argon gas.

Table 1. Etch Depths Required for Binary and Four-Level Phase BCGH Made of Lithium Niobate

	Binary Phase BCGH		Four-Phase-Level BCGH	
Φ_o, Φ_e	d_1 (μm)	d_2 (μm)	d_1 (μm)	d_2 (μm)
0, 0	1.475	1.475	2.213	2.213
0, $\pi/2$			1.475	2.900
0, π	0.000	2.850	0.7375	3.587
0, $3\pi/2$			0.000	4.275
$\pi/2$, 0			2.900	1.475
$\pi/2$, $\pi/2$			2.162	2.162
$\pi/2$, π			1.425	2.112
$\pi/2$, $3\pi/2$			0.687	3.690
π, 0	2.850	0.000	3.587	0.7375
π, $\pi/2$			2.850	1.425
π, π	1.375	1.375	2.112	2.112
π, $3\pi/2$			1.375	2.800
$3\pi/2$, 0			4.275	0.000
$3\pi/2$, $\pi/2$			3.537	0.687
$3\pi/2$, π			2.800	1.375
$3\pi/2$, $3\pi/2$			2.062	2.062

The etch depth of each fabricated surface relief was measured by a Dektak IIA surface profiler. Figure 4 shows an example of a linear scan of such a profile of a four-phase-level BCGH. We calculated the algebraic average etch depth $\bar{d}$ by selecting ten data points at random from the measured results. The etch uniformity U is defined as the ratio

$$U = \frac{\max(|d_i - \bar{d}|)}{\bar{d}}, \tag{17}$$

where max defines the maximum value operation and d_i is the randomly chosen measured etch depth at $i = 1, 2, \ldots, 10$ sampling points. For the BCGH elements that were fabricated we found that the accuracy of the measured etch depth was within 3% of its designed value with etch uniformity better than 5%.

When the etching process was completed, the etched 1 in. × 2 in. (25 mm × 51 mm) lithium niobate wafer was cut into two 1 in. × 1 in. (25 mm × 25 mm) substrates. To complete the fabrication, we had to assemble the substrates with the surface-relief patterns aligned and in contact. We considered and used two methods. The first used a standard microlithography mask aligner, while the second used an *in situ* optical alignment and testing setup constructed on an optical benchtop. The basic procedure for both assembly methods is shown schematically in Fig. 5. We made the etched substrates easier to handle by temporarily bonding them to microscope slides with a transparent heat-release glue (Aremco Crystalbond 509). The substrates are aligned in the mask aligner or the *in situ* assembly setup, and then UV curing epoxy (Loctite Chipbond 346) is applied around the edges of the two lithium niobate plates. After a final fine alignment, the epoxy is cured by UV light. Finally, the assembled BCGH is released from the glass substrates by heating. The residue of the heat-release glue is removed by acetone.

For assembly with the mask aligner we added alignment marks (e.g., cross and diamond pairs) to the *e*-beam mask. These marks were ion etched into the hologram substrates during the fabrication process. When the substrates were brought into contact, the patterns on both the upper and lower substrates were clearly visible. The substrates could be aligned to within 2 μm, the accuracy of our mask aligner.

The second approach was *in situ* alignment. Here the two substrates were held in an optical setup that permitted them to be illuminated with a collimated laser beam during alignment. The efficiency and polarization contrast ratio of the holographic reconstruction could be measured in real time with an optical detector or a CCD camera. BCGH performance was maximized with high-resolution translation and rotation stages (total of six degrees of freedom) before the two substrates were bonded. As an alternative to measuring hologram performance, we also designed additional alignment features such as gratings, incorporated in the *e*-beam mask. These features generated Talbot images and moiré patterns, which could be interpreted and used to guide accurate alignment.

In principle, *in situ* alignment should permit maximum performance. In practice, however, we found that, while excellent BCGH performance could be observed before curing the epoxy, performance was not maintained after curing. The apparent source of this problem is the shrinkage of the epoxy during curing. This could be cured by ensuring a fully

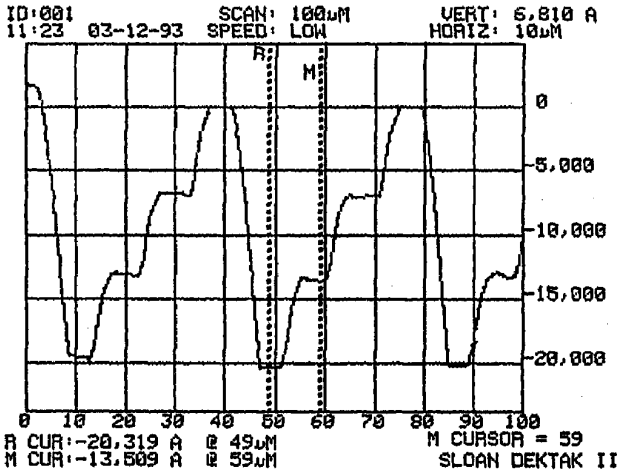

Fig. 4. Surface-reflief profile of an ion-milled $LiNbO_3$ substrate measured by a Dektak profilometer.

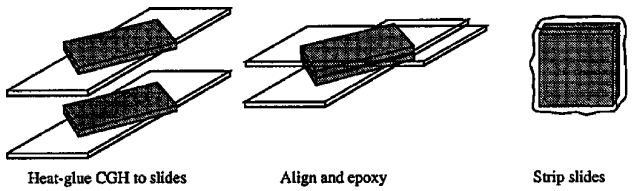

Fig. 5. Schematic diagram describing the BCGH assembly procedure.

uniform epoxy thickness to equalize stresses, or more simply, by identifying a UV curing epoxy that maintains equal volume during curing. The mask aligner, which held the two substrates in tight contact during curing, did not seem to be as prone to this problem.

There are two dominant optical losses in a BCGH: surface reflections and diffraction loss (light diffracted into other than the first order). While lithium niobate has a high birefringence, it also has a large index of refraction (~2.3), which causes ~16% loss at each of the four surfaces. In addition to reducing transmission efficiency, this can increase background noise and reduce the polarization contrast ratio. To minimize these losses, we had an etched unassembled BCGH substrate coated with a single-layer antireflection (AR) coating with a silicon dioxide (SiO_2) thin film (thickness $\lambda/4$ at $\lambda = 514.5$ nm) by use of an ion-plating evaporation system. The reflectance of the AR-coated single substrate of lithium niobate was measured to be $0.4 \pm 0.1\%$. Compared with uncoated BCGH, the reflection loss is reduced from 49% to less than 1%. Figure 6 shows the reflectance of a lithium niobate substrate with both sides AR coated, as a function of wavelength.

5. Experimental Results and Applications

A. Experiment Evaluations of the Birefringent Computer-Generated Holograms

Four different holograms were made: (1) a simple polarizing beam splitter (PBS), to deflect one polarization and to transmit the other, (2) a dual PBS, to deflect one polarization vertically and the other horizontally, (3) a dual cylindrical lens, to focus the two orthogonal polarizations into a vertical or horizontal line, and (4) a dual spherical lens, with a focal length of f and $2f$ for vertically and horizontally polarized light, respectively. Each hologram was 5 mm × 5 mm, with a design wavelength $\lambda = 514.5$ nm. The focal lengths ($f = 100$ mm, for $F/20$) and deflection angles (1.5°) were chosen to produce a grating period of at least 20 μm, corresponding to a minimum feature size of 10 μm. Kinoform patterns were calculated and converted to binary phase for each polarization. Then the two kinoforms were combined to produce mask patterns for two etches of 1.37 and 1.47 μm. Chrome masks were generated by electron-beam lithography and transferred to a photoresist on the substrates by contact-print lithography.

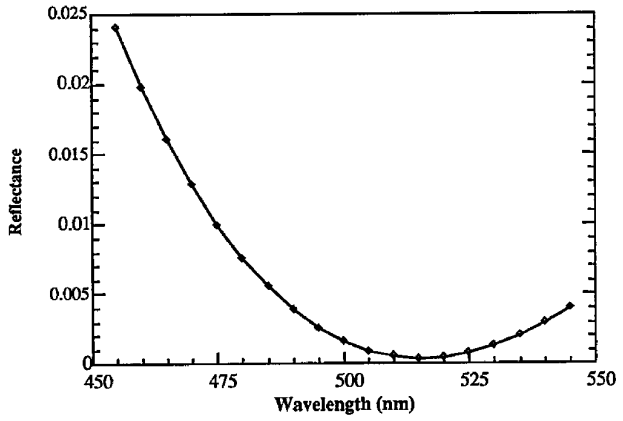

Fig. 6. Reflectance of AR-coated $LiNbO_3$ substrate.

All of the BCGH's were polarization selective, as expected. For BCGH characterization we measured the maximum first-order diffraction efficiency η, defined as the intensity ratio of the first diffracted order over all the transmitted orders, and the polarization contrast ratio R, defined as the ratio between the diffracted light intensities at ordinary and extraordinary polarizations. The measured characteristics of the four holograms were as follows: for the simple polarizing beam splitter (PBS), $\eta = 25\%$ and $R = 10{:}1$; for the dual polarizing beam splitter, $\eta = 6\%$ and $R = 40{:}1$; for the dual cylindrical lens, $\eta = 20\%$ and $R = 6{:}1$, for the dual spherical lens, $\eta = 17\%$ and $R = 6{:}1$. These efficiencies were significantly less than the theoretical maximum first-order efficiency for a binary phase grating of 40.5%. Less than 0.2% of the intensity was lost into the zeroth order for the dual PBS, however, indicating that the proper etch depths were obtained.

To increase the diffraction efficiency, we fabricated a multilevel phase (four-level) BCGH. This doubles the theoretically achievable diffraction efficiency to 80.5%. The BCGH element was designed for application in a multistage interconnection network consisting of 16 nodes, and it consisted of a 4 × 4 array of blazed gratings. The grating periods are 40 μm, while the smallest feature size in the hologram is 10 μm, which is the same as that used in our binary phase holograms. The performance was increased to a measured diffraction efficiency of 26.3% and a contrast ratio of 130:1 with a new four-level phase element. More recently, a repeated fabrication of the four-level phase element yielded an increased diffraction efficiency of 60% with a contrast ratio of 160:1. This is the best result to date.

The reconstruction of the fabricated BCGH is obtained by illumination of the BCGH element with a collimated argon-ion laser beam at 514.5 nm. Tilting the element relative to the input beam affected the efficiency and contrast. The optimum performance was found (and measured) at nonzero incidence angles. This was apparently an effect of fabrication and assembly errors. The optimum angle that gave the maximum diffraction efficiency was ~40°, and the angles were slightly different (~5°) for the two orthogonal polarizations. If the readout angle was fixed at an intermediate angle, the average diffraction efficiency was 45% with a 120:1 contrast ratio.

Alignment errors included misalignment between the multiple etched patterns and between the two etched surfaces during final assembly of two BCGH substrates as well as misalignment of the two BCGH substrates' crystal optic axis. Etching errors include depth inaccuracy (under- and over-etching) as well as nonvertical sidewalls. Slanted (V-shaped-groove) sidewalls have been observed in ion-etched lithium

niobate.[13] This effect also changes the duty cycle of the grating.

The ideal diffraction efficiency of a single-substrate diffractive grating has been predicted with various models.[8,14–16] Alignment errors are impossible to avoid, but they can be significantly reduced with the use of a state-of-the-art aligner. Here, we adopt the analysis performed by Cox *et al.*[17] and Farn and Goodman[18] on the influence of fabrication-induced errors on the diffraction efficiency of a single-substrate diffractive optical element. One potential source of inaccuracy was the etching process. The under- and over-etch errors are controlled within 3% with a 5% etching uniformity for all of our fabricated BCGH elements. Therefore the desired phase function of the BCGH is affected by a random-varying function in space with magnitude less than 5%. Both Refs. 13 and 14 show that the degradation of diffraction efficiency depends quadratically on the etching errors. A 5% etching error introduces only a 1% diffraction-efficiency degradation. We calculated the effect of sloping sidewalls on the diffraction efficiency of a binary phase single-substrate grating by computing and summing the Fourier coefficients of such a grating. The results indicate that the sidewall slopes on our fabricated elements did not cause significant degradation of diffraction efficiency.

Another source of fabrication error is alignment. The calculations of Ref. 13 show that, when the 40-μm zone spacing of a Fresnel zone plate is slightly altered, with an alignment error of 0.5 μm, the diffraction efficiency will drop from the ideal 81% to ~75%.[13] The diffraction efficiency is linearly related to the alignment errors.[14] The feature size of four BCGH is 10 μm, while the alignment accuracy of our mask aligner and assembly process are both ~2 μm. A misalignment of 2 μm results in a theoretical diffraction efficiency of 65% rather than the originally predicted 81%. This seems to explain the 60% efficiency of our fabricated four-phase-level BCGH elements and indicates a profitable direction for improving the fabrication process.

B. Application of the Birefringent Computer-Generated Hologram for Image Processing

BCGH elements apply an arbitrary and independent (computer-designed) phase profile to each input polarization. Such phase holograms may have diffraction efficiencies approaching 100%. This capability immediately suggests applications in monochromatic optical systems, for example, as a lightweight readout head for fast-access magneto-optic optical-disk storage.[19] Even more interesting applications arise when BCGH's are combined with active polarization rotating modulators such as electro-optic lead lanthanum zirconated titanate[20] and liquid-crystal[21] modulators. The combination permits direct electrical control of an optical system without introducing moving parts. For example, a solid-state zoom lens could be designed to switch between multiple discrete positions with a microsecond time response.

For BCGH to become practical for such applications it will be important to achieve high diffraction efficiency and to reduce the minimum feature size. However, it is already possible to begin making prototype optical systems to demonstrate their potential. We have fabricated BCGH elements suitable for two applications: image processing and free-space optical interconnection networks.

The two basic functions of a lens are imaging and performing a spatial Fourier transform. We designed and fabricated a BCGH holographic lens with dual focal lengths for the two orthogonal linear polarizations where the focal length f_h, for horizontal polarization, was 200 mm, while focal length f_v, for vertical polarization, was 100 mm. We designed and fabricated a binary phase on-axis holographic lens, as described in Section 4.

When this element is placed 200 mm from an input transparency, then the output plane 200 mm beyond the BCGH should contain either the image or the Fourier transform of the input image, depending on input light polarization [see Fig. 7(a)]. If a large-aperture polarization rotator is placed in front of the BCGH, then the output can be switched between the two states, depending on whether the polarization is rotated or not [see Fig. 7(a)]. Figures 7(b) and 7(c) show the experimental result for this system. Figures 7(b) and 7(c) are the image and the spatial Fourier transform of the inverse of the characters UCSD, respectively. Only slight cross talk between the Fourier transform and the zero order can be seen in the image.

C. Application of the Birefringent Computer-Generated Hologram as a 2 × 2 Optical Switch for Interconnection Networks

Figure 8 shows how two BCGH's and an electro-optic polarization rotator can be used to construct a binary 2 × 2 optical switch. The first hologram combines and focuses the two inputs into the modulator, which either exchanges their polarizations or not. The second hologram separates and directs the outputs to their destinations. For example, an optoelectronic multistage interconnection network (MIN) would consist of a series of two-dimensional arrays of such switches. The advantage of focusing the light through small aperture is that it reduces the modulation area, so that smart-pixel arrays with local electronic processing can be used to control network routing.

To demonstrate the concept, we used the two planar-polarizing beam-splitter BCGH holograms (without the focusing and output deflection capabilities) that were described in Section 5. The schematic diagram of our optical setup is shown in Fig. 9(a). To simulate two data channels, two beam choppers modulated two orthogonally polarized input beams at different frequencies. The two modulated beams propagating in different directions at the input are combined by the first BCGH element, and both propagate in the same direction through a liquid-

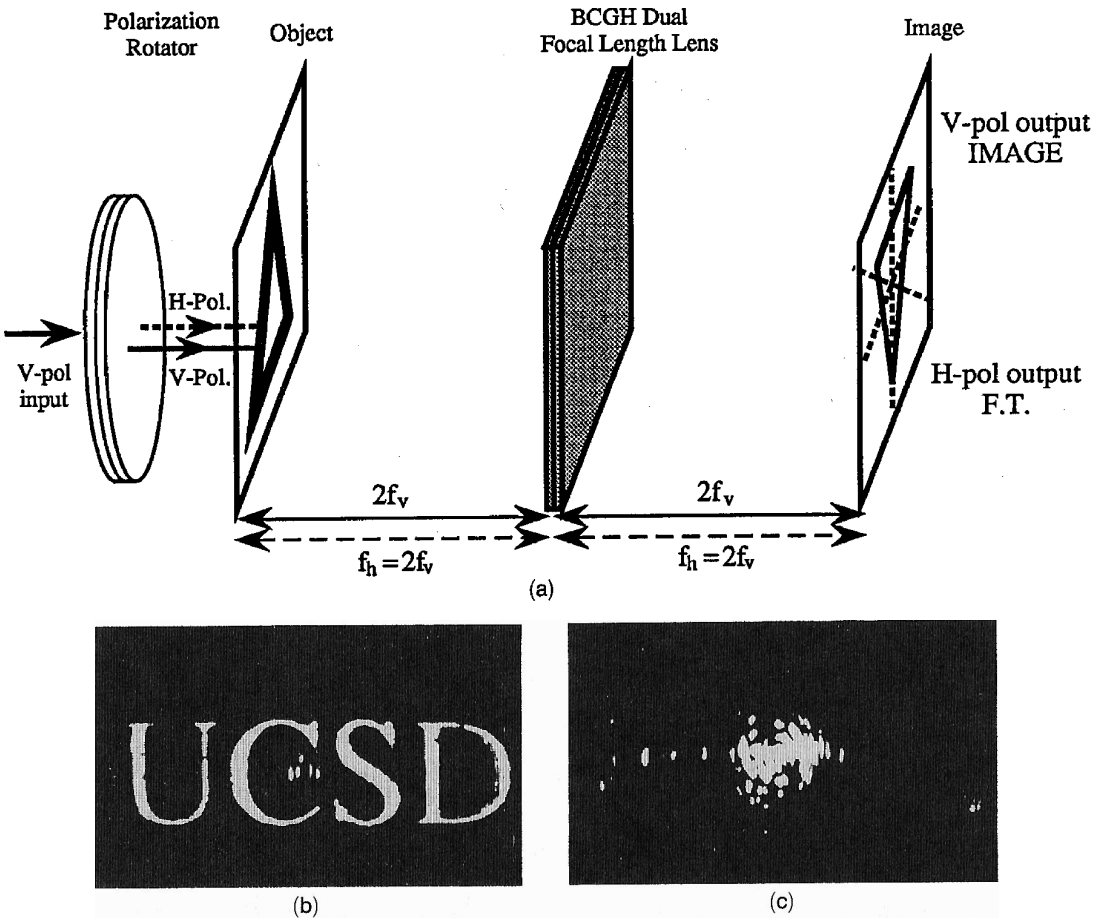

Fig. 7. Imaging and Fourier transforming at the same plane without any moving parts: (a) schematic diagram of the experimental setup, (b) photograph of the image of the object obtained with vertical polarization, and (c) photograph of the spatial Fourier transform of the object obtained with horizontal polarization.

crystal (LC) polarization rotator. The second BCGH element deflected the two transmitted beams into different directions to be detected by two photodetectors. If the LC is off, the two beams propagate straight through. When the LC is turned on, the polarizations of the two beams are switched, and the outputs are detected at opposite detectors. In our demonstration we applied a square-wave voltage to the LC, causing periodic switching of the light beams between the two output photodetectors. The oscilloscope traces shown in Fig. 9(b) show the switching of information between the two output channels.

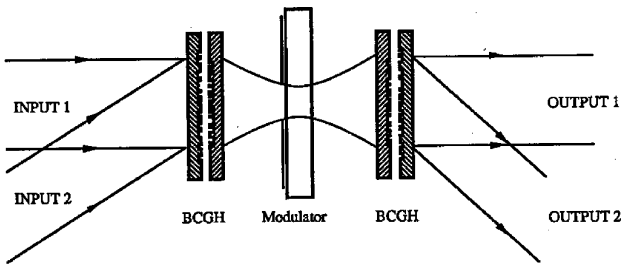

Fig. 8. Principle of a 2 × 2 optically routing polarization switch using a BCGH.

The switching speed of the 2 × 2 switch is limited by the polarization-rotator response time. In our demonstration a liquid-crystal polarization rotator was operated at a switching rate of ~1 kHz. If we use a lead lanthanum zirconated titanate or a multiple-quantum-well (MQW) based polarization rotator, switching as fast as 10–100 MHz might be achieved.[22,23] Such a polarization-selective optical switch may be used to build a MIN where simple binary switches are arranged into many layers. This type of MIN may provide effective and efficient interconnection for large communication networks. We can design a circuit-switched optical MIN using binary polarization switches and polarization-selective CGH's to switch and route the light at each node. The network setup time (latency) would depend on the modulator technology, but the data modulation rate would be limited only by the input sources. This rate could easily exceed 1 GHz, and may approach terahertz as telecommunication technology advances. Polarization-selective CGH's permit the network to be simple and compact, because each hologram would replace an entire subsystem of component required to build the network with conventional optics. More information about BCGH MIN

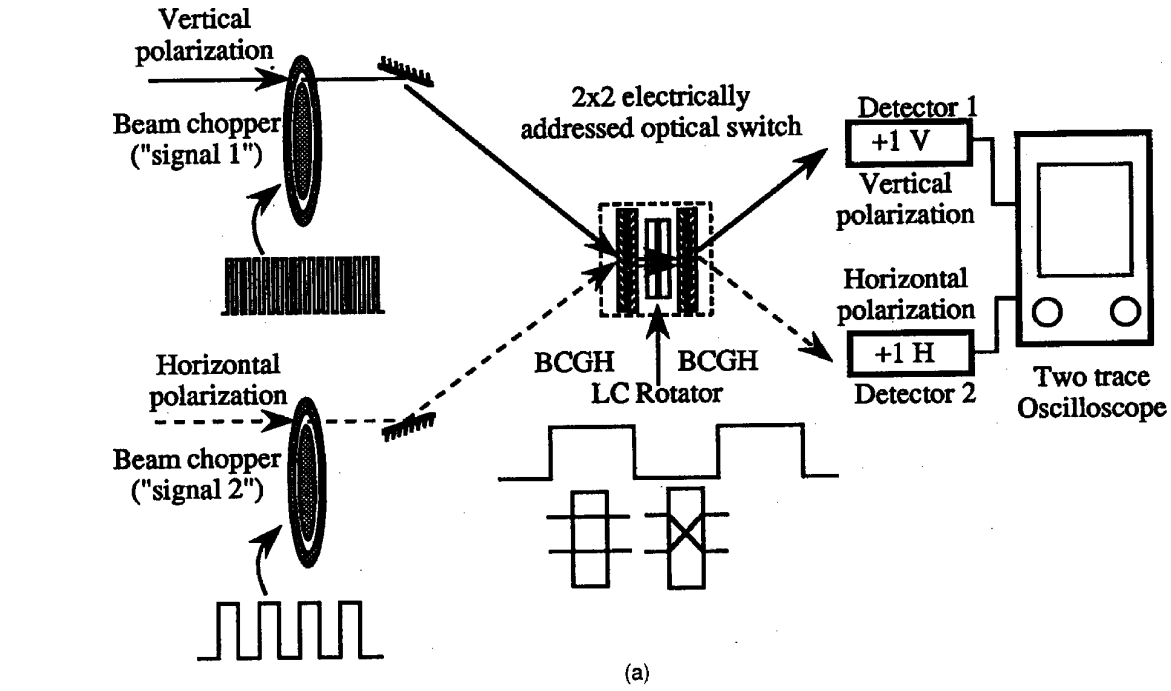

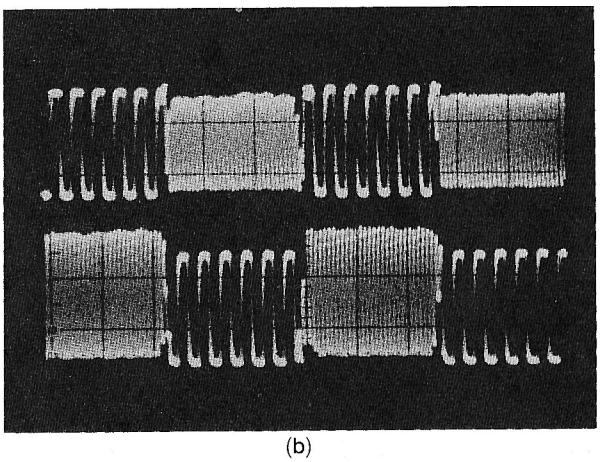

Fig. 9. 2×2 switch demonstration: (a) schematic diagram of the experimental setup, (b) photograph of the oscilloscope trace demonstrating switching.

network design and more advanced experimental results will be described in the future.

Another potentially significant application of BCGH is the packaging of optoelectronic devices and systems. Such systems often use CGH for beam forming (spot array generation) and optical interconnection between planes of processing-element arrays.[24] A single BCGH replaces two conventional holograms and avoids the weight and volume of the polarizing cube beam splitter. Optical alignment and system assembly are two of the more difficult tasks in constructing working systems. A major advantage of BCGH's for these applications is that the widely spaced conventional CGH's are combined into a single prealigned planar component that can be located close to the processor array, dramatically simplifying alignment and potentially increasing system reliability.

6. Conclusions

This paper has described the design, fabrication, and testing of polarization-selective CGH elements that are composed of two surface-etched birefringent substrates joined face to face. We showed the design methodology for multilevel phase holograms constructed from arbitrary birefringent substrate and gap materials. Using standard microelectronics methods, we have fabricated holograms with 60% diffraction efficiency and >100:1 polarization contrast ratios. While this performance is far from the theoretical maximum, we have considered the effects of etching and alignment errors, and we believe that near-optimum performance is possible. We have also shown that a single-layer SiO_2 thin-film antireflection coating on all surfaces can reduce reflections from the high-index substrates without a significant effect on hologram performance. This means that holograms with very large (500:1) polarization contrast ratios and efficiencies approaching 100% are possible.

We have also investigated some possible applications of this technology. We demonstrated experimentally a dual focal-length lens for image processing

and a self-interconnecting binary 2 × 2 polarization switch suitable for a transparent optical multistage interconnection network. Finally, we have discussed the possible role of polarization-selective CGH's in building compact optoelectronic components and systems.

Our future research goals are directed toward reducing the cost of two-substrate BCGH's with birefringent polymers and other low-refractive-index and high-birefringence substrates, and toward developing a single-substrate BCGH with increased spatial resolution with either form birefringence or surface deposition of birefringent layers.

The authors thank Brian Sullivan and Allan Waldorf of Canada's National Research Council for their optical coatings and Bob Tekolste at Hughes Aircraft Company for the loan of two liquid-crystal polarization rotators. We also thank our colleagues Sadik Esener, Sing Lee, Walter Däshner, Jian Ma, Volkan Ozguz, Kris Urquhart, Rob Stein, and especially Ashok Krishnamoorthy for their valuable contributions. This work was supported by the National Science Foundation under grant ECS-9311062, the Advanced Research Projects Agency under grant OTCII-MDA 972-94-1-002, NATO under grant HTECH-CRG-931141, and the U.S. Air Force under grant F-30602-91-C-0094.

References and Notes

1. T. Todorov, L. Nikolova, K. Stoyanova, and N. Tomova, "Polarization holography. III. Some applications of polarization holographic recording," Appl. Opt. **24,** 785–788 (1985).
2. Q. W. Song, M. C. Lee, and P. J. Talbot, "Polarization sensitivity of birefringent photorefractive holograms and its applications to binary switching," Appl. Opt. **31,** 6240–6246 (1992).
3. R. Kostuk, M. Kato, and Y. T. Huang, "Polarization properties of substrate-mode holographic interconnects," Appl. Opt. **29,** 3848–3854 (1990).
4. K. Yokomori, "Dielectric surface-relief gratings with high diffraction efficiency," Appl. Opt. **23,** 2303–2310 (1984).
5. H. Haidner, P. Kipfer, J. Sheridan, J. Schwider, N. Streibl, J. Lindolf, M. Collischon, A. Lang, and J. Hutfless, "Polarizing reflection grating beams splitter for the 10.6-μ wavelength," Opt. Eng. **32,** 1860–1865 (1993).
6. A. Ohba, Y. Kimura, S. Sugama, Y. Urino, and Y. Ono, "Holographic optical element with analyzer function for magneto-optical disk head," Jpn. J. Appl. Phys. Suppl. **28,** 359–361 (1989).
7. J. Hoßfeld, D. Columbus, H. Sprave, T. Tschudi, and W. Dultz, "Polarizing computer-generated holograms," Opt. Eng. **32,** 1835–1838 (1993).
8. G. S. Swanson, "Binary optics technology: the theory and design of multilevel diffractive optical elements," MIT Lincoln Laboratory Tech. Rep. 854, (MIT, Cambridge, Mass., 1989).
9. M. Born and E. Wolf, *Principle of Optics,* 6th ed. (Pergamon, New York, 1989), pp. 705–708.
10. P. Kipfer, M. Collischon, H. Haidner, J. T. Sheridan, J. Schwider, N. Streibl, and J. Lindolf, "Infrared optical components based on a microrelief structure," Opt. Eng. **33,** 79–84 (1994).
11. Lithium niobate optical crystal data sheet (Crystal Technology, Inc., Palo Alto, Calif., 1992).
12. C. Pitt, M. Fraser, N. Polozkov, and L. Ivleva, "Growth and materials processing of $LiNbO_3$," in *Properties of Lithium Niobate,* EMIS Datareview Series No. 5 (INSPEC, Institution of Electrical Engineers, London, 1989), pp. 205–236.
13. R. E. Chapman, "Argon and reactive ion beam etching for SAW devices," Vacuum **34,** 417–424 (1984).
14. H. Dammann, "Blazed synthetic phase-only holograms," Optik **31,** 95–104 (1970).
15. U. Krackhardt, N. Streibl, and J. Schwider, "Fabrication errors of computer generated multilevel phase holograms," Optik **95,** 137–146 (1994).
16. T. Gaylord and M. Moharam, "Analysis and applications of optical diffraction by gratings," IEEE Proc. **73,** 894–937 (1985).
17. J. Cox, T. Werner, J. Lee, S. Nelson, B. Fritz, and J. Bergstrom, "Diffraction efficiency of binary optical elements," in *Computer and Optically Formed Holographic Optics,* J. Cindrich and S. H. Lee, eds., Proc. Soc. Photo-Opt. Instrum. Eng. **1211,** 116–124 (1990).
18. M. W. Farn and J. W. Goodman, "Effect of VLSI fabrication errors on kinoform efficiency," in *Computer and Optically Formed Holographic Optics,* J. Cindrich and S. H. Lee, eds., Proc. Soc. Photo-Opt. Instrum. Eng. **1211,** 125–136 (1990).
19. A. Ohba, Y. Kimura, S. Sugama, R. Katayama, and Y. Ono, "Reflection polarizing holographic optical element for compact magneto-optical disk heads," Appl. Opt. **29,** 5131–5135 (1990).
20. C. J. Kirkby, M. J. Goodwin, and A. D. Parsons, "PLZT/silicon hybridized spatial light modulator array: design, fabrication, and characterization," Intl. J. Optoelectron. **5,** 169–178 (1990).
21. L. K. Cotter, T. J. Drabik, R. J. Dillon, and M. A. Handschy, "Ferroelectric-liquid-crystal/silicon-integrated-circuit spatial light modulator," Opt. Lett. **15,** 291–293 (1990).
22. C. J. Kirkby, "Electro-optic switching response in cubic phase PLZT ceramic materials," Appl. Opt. **15,** 828–830 (1976).
23. M. Wraback, H. Shen, J. Pamulapati, M. Dutta, P. Newman, and Y. Lu, "Femtosecond studies of ultrafast large-angle polarization rotation in $GaAs/Al_xGa_{1-x}As$ multiple quantum wells under uniaxial stress," in *Quantum Optoelectronics,* Vol. 8 of 1993 OSA Technical Digest Series (Optical Society of America, Washington, D.C., 1993), pp. 98–99.
24. F. B. McCormick, T. J. Cloonan, F. A. Tooley, A. L. Lentine, J. M. Sasian, J. L. Brubaker, R. L. Morrison, S. L. Walker, R. J. Crisci, R. A. Novotny, S. J. Hinterlong, H. S. Hinton, and E. Kerbis, "Six-stage digital free-space optical switching network using symmetric self-electro-optic-effect devices," Appl. Opt. **32,** 5153–5171 (1993).